Departures from convective equilibrium with a rapidly-varying surface forcing

L. Davies[a*] and R. S. Plant[a] and S. H. Derbyshire[b]
[a]*Department of Meteorology, University of Reading, Reading, UK*
[b]*Met Office, Exeter, UK*
*Correspondence to: School of Mathematical Sciences, Monash University, Melbourne, Australia. E-mail: laura.davies@monash.edu

Convective equilibrium is a long-standing and useful concept for understanding many aspects of the behaviour of deep moist convection. For example, it is often invoked in developing parameterizations for large-scale models. However, the equilibrium assumption may begin to break down as models are increasingly used with shorter timesteps and finer resolutions. Here we perform idealized cloud-system resolving model simulations of deep convection with imposed time variations in the surface forcing. A range of rapid forcing timescales from $1-36$hr are used, in order to induce systematic departures from equilibrium. For the longer forcing timescales, the equilibrium assumption remains valid, in at least the limited sense that cycle-integrated measures of convective activity are very similar from cycle to cycle. For shorter forcing timescales, cycle-integrated convection becomes more variable, with enhanced activity on one cycle being correlated with reduced activity on the next, suggesting a role for convective memory. Further investigation shows that the memory does not appear to be carried by the domain-mean thermodynamic fields but rather by structures on horizontal scales of $5-20$km. Such structures are produced by the convective clouds and can persist beyond the lifetime of the cloud, even through to the next forcing cycle. Copyright © 0000 Royal Meteorological Society

Key Words: cloud-resolving modelling; convective quasi-equilibrium; rapid forcing

Received ¡Article history¿

Citation: . . .

1. Introduction

One of the limitations of general circulation models, and most numerical weather prediction models, is the necessity for convective processes to be represented through a parameterization. A key issue in convective parameterization is the so-called "closure problem", essentially the specification of the strength of the sub-grid scale convective activity for a given grid-scale state. Following Arakawa and Schubert (1974), a common assumption made to determine the closure is that the convection acts as a counterbalance to the large-scale forcing, thereby maintaining the atmosphere close to a state of equilibrium. This equilibrium assumption is often highlighted as one of the main limitations of convective parameterizations (e.g. Mapes 1997; Arakawa 2004; Zimmer *et al.* 2011), especially for the problem of the diurnal cycle of convection (e.g. Yang and Slingo 2001; Guichard *et al.* 2004). The issue is increasingly brought to the fore by the progress being made towards higher resolution models, run with shorter timesteps, and it may well be that departures from equilibrium should be systematically taken into account. As discussed below, several methods for doing so have been proposed in the literature. Here we will perform cloud-system resolving model (CRM) experiments that are designed to test the range of validity of the equilibrium assumption and to reveal processes that may be important for the description of out-of-equilibrium behaviour.

The assumption of convective quasi-equilibrium is often interpreted in terms of a timescale separation between the relatively fast evolution of the convection and the slow

evolution of the large-scale convective forcing. The large-scale forcing occurs through non-convective processes that tend to increase convective instability (however measured). In practice, such a separation between convective and non-convective processes is hardly clear-cut (Mapes 1997), but the forcing may nonetheless be considered as well-defined in many idealized CRM experiments by means of an experimental design that essentially fixes those processes producing instability. Just such an approach will be followed here.

Even if exact equilibrium were to hold, any data analysis conducted for a finite-size domain will of course exhibit random fluctuations arising from the limited sampling. However, systematic departures from an exact equilibrium will also occur: first, because the large-scale forcing does vary in the real atmosphere; and, second because the response of convection to a given forcing requires a finite adjustment time rather than being instantaneous. Thus, convection depends "on the past history of the large-scale forcing, but ... only within the timescale of adjustment" (Arakawa and Schubert 1974, p691). The adjustment timescale was argued by Arakawa and Schubert (1974) to be at least as long as the lifecycle of an individual cumulus cloud that is triggered in response to the forcing prevailing at that time. Following a step-change in forcing amplitude, Cohen and Craig (2004) showed that the adjustment timescale scales with the inter-cloud spacing, consistent with the gravity-wave mechanism proposed by Bretherton and Smolarkiewicz (1997). Other adjustment scalings have also been proposed, such as that from the similarity theory of Grant and Brown (1999).

If translated strictly into a convective parameterization, an exact convective equilibrium would imply that the convection should fully adjust the atmosphere to the current forcing at each model timestep. Such an approach was used in some early studies (e.g. Manabe *et al.* 1965), but as it is unlikely that large, complex, convective systems would complete a lifecycle in a model timestep, modern parameterizations explicitly recognize a non-zero adjustment time, generally in the form of a closure which seeks to relax the atmosphere to a neutral state over the course of a "closure timescale" (e.g. Gregory 1997; Kain 2004). The choice of the closure timescale can have important effects on the behaviour of the parent model (e.g. Bechtold *et al.* 2008), indicating that departures from equilibrium are well worthy of investigation. The use of a closure timescale partially addresses departures from an exact convective equilibrium, but does not address the presence of feedback in convective systems. How, and in what circumstances, do on-going convective processes modify subsequent convective events?

The use of a closure timescale does not directly account for the effects of previous convection in modifying current convective intensity. This feedback process is referred to as memory in this paper. Some convective parameterization schemes have considered prognostic terms in their closure formulations. One approach (Pan and Randall 1998; Wagner and Graf 2010; Yano and Plant 2012) is formulated around the convective energy cycle system of Arakawa and Schubert (1974), while another is based on a consideration of the moist static energy budget (Gerard and Geleyn 2005). Other treatments of memory have focussed on microphysical mechanisms, most notably the separation of dynamics and microphysics by Piriou *et al.* (2007) and the recent study by Mapes and Neale (2011) who introduced "organisation" parameter driven by rain reevaporation which is used to modify the entrainment rate and closure. It is also worth noting closures that have been proposed based on assumptions about related boundary-layer processes rather than requiring a convective equilibrium. Examples include Bretherton *et al.* (2004), based on an assumed pdf of vertical velocity at the inversion level, and Rio *et al.* (2009); Grandpeix and Lafore (2010), who estimate an available lifting power induced by boundary layer thermals and convective wakes.

Davies *et al.* (2009) investigated a simple dynamical system which may provide an idealized model of convection with memory effects. The system is essentially a reinterpretation of the prognostic system of Pan and Randall (1998) but with its response studied for an imposed periodic forcing. Davies *et al.* (2009) demonstrated that the convective response could be characterised by qualitatively distinct regimes, depending upon the chosen memory timescale and the period of the imposed forcing. In the current study we seek to investigate whether a fully realistic convective system can behave in a similar manner, by performing simulations with a CRM. Of course, the memory timescale cannot be chosen in such a model but rather is established by the complex behaviour of the simulated flow. The forcing, however, is prescribed in the CRM, and by applying a periodic forcing with various different periodicities we can look for any qualitative changes of regime. The aim is to establish the circumstances under which memory becomes an important consideration in describing the convection.

Convection can readily become organized in the presence of rotation or wind shear (e.g. Rotunno *et al.* 1988; Vallis *et al.* 1997; LeMone *et al.* 1998; Robe and Emanuel 2001). This study has been conducted for a non-rotating atmosphere with no imposed wind. Thus, any organization in the simulated convection will be self-organization and the convective ensemble will be as similar as possible to the random configuration that is normally assumed by a parameterization. This is in contrast to the interesting recent investigation by Jones and Randall (2009) which is similar in the sense that rapid time variations in the forcing are considered, but dissimilar in the sense that prominent mesoscale organization develops in some of the Jones and Randall (2009) simulations in response to an imposed shear (see also Sec. 5 of Jones (2010)). The strength of the mesoscale organization is an important factor in explaining differences within that set of simulations.

This paper is structured as follows. In Section 2 we discuss some relevant aspects of Davies *et al.* (2009), highlighting in particular the regimes of interest and the form of the forcing, which motivate the experimental design followed here. The CRM experiments are detailed in Section 3 and are analysed in Section 4 by contrasting the convective response for a range of forcing timescales. A summary and conclusions can be found in Section 5.

2. Characterizing convection with memory

Davies *et al.* (2009) considered an idealized analytic model of convection for an atmosphere being radiatively cooled at a prescribed constant rate above a surface with a prescribed, time-varying temperature. The functional form of the time-variation was chosen as an idealization of the diurnal cycle over land. Specifically the surface temperature was held

fixed for half of the forcing cycle and increased by the positive part of a sinusoid for the other half.

The model identifies two timescales that control the convective response: a closure timescale governing the removal rate of instability in the presence of a steady forcing; and, a memory timescale governing the response to variations in the forcing. The closure timescale is similar to that used in many convective parameterizations. The memory timescale was included as a crude representation of the lifecycle of convection. It determines the rate at which the convective heating is adjusted in response to a change of forcing and provides a feedback from the previous rate of convective heating to the current heating. A non-linear aspect to the system arises from a requirement that the surface temperature exceeds the atmospheric temperature in order for convection to be active.

After allowing a few forcing cycles for initial transients to die away, the results were classified into various regimes of convective behaviour, depending upon the values of the memory timescale, the closure timescale and the forcing timescale. Two regimes were found in which the convection was highly repetitive and predictable. If the memory timescale is short compared to the forcing timescale then the convection follows the pattern of the forcing and the same time-integrated convective heating occurs on each cycle. Such behaviour corresponds to a situation in which convective quasi-equilibrium holds good. Conversely, if the memory timescale is long compared to the forcing timescale then the convective heating is almost steady with only small fluctuations being induced by the rapid variations in forcing. In other words, the memory strongly dampens very fast variations in the forcing.

However, a rather different regime occurs if the memory and forcing timescales are similar. The convection can then be highly variable from one cycle to the next, some forcing cycles having strong convective heating, others with relatively little and still others being skipped entirely. In this regime the lifecycle of convective cloud, as represented by the memory timescale, has a clear effect in modifying the subsequent convective response. The regime seems to have no direct analogies with the documented behaviour of current convective parameterizations.

The above regimes could be produced by fixing values for the memory and closure timescales and varying the forcing timescale. This point is useful for our present study as it provides a way to investigate whether simulated convection exhibits similar regimes. In the remainder of this paper, we will compare CRM experiments subjected to a very similar pattern of convective forcing, and for which different forcing timescales have been imposed. In this way we will determine whether, and in what circumstances, a convective ensemble behaves as a system for which memory plays an important role. Moreover, we will consider the possible physical origin of memory effects in convective ensembles.

3. Model details and experimental design

3.1. Model details

The numerical model used for this study is the Met Office Large Eddy Model (LEM). Details of the model that are important for the experiments performed here are described below, while a full presentation of the model is available from Shutts and Gray (1994); Gray *et al.* (2001). The model solves the primitive equations with anelastic, quasi-Boussinesq approximations which allow for variations with height of reference profiles of pressure, temperature and density. This is an appropriate approximation for convective systems where the buoyancy of clouds is defined by density perturbations. The LEM represents three-phase microphysics using prognostic equations for the single-moment mixing ratios of water vapour, liquid water and rain, and for double-moment mixing ratios and number concentrations for the ice variables (ice, snow and graupel). The sub-grid scheme parameterizes the small dissipative eddies which are not explicitly resolved in the model based on a diagnostic Smagorinsky-Lilly approach, which has no explicit memory in the representation of small-scale turbulence.

The model is run in three dimensions over a horizontal domain that is biperiodic and of area $(64\text{km})^2$. It has been argued that a three dimensional model is necessary to simulate cold pool dynamics (Tompkins 2001) and gravity wave propagation (Bretherton and Smolarkiewicz 1997). Such dynamical mechanisms may provide suitable candidates for contributing to an element of memory in the system, since the mechanisms can persist beyond the lifecycle of the cloud that initially induces the dynamics.

The horizontal grid length is 1km, which is coarser than that required to represent the transition from shallow to deep convection (e.g. Petch 2006) but the focus here is on the deep convection itself rather than details of the transition to it. Some test integrations on larger domains showed that the results to be presented here are not qualitatively sensitive to the domain size (Davies 2008). Jones and Randall (2009) also performed a range of simulations to investigate departures from quasi-equilibrium and used a larger grid but a coarser horizontal resolution. The experimental setup of Jones and Randall (2009) included a prescribed wind shear, which results in mesoscale organization that can be captured with the larger domain. Given the setup chosen here, without wind shear or rotation, no such large-scale organization of the cloud field occurs (see Section 4.5) and so a more modest domain size is adequate.

The vertical domain is a stretched grid with 76 levels. The level spacing is 25m close to the surface, around 50m through the bulk of the boundary layer, 250m in the free troposphere and 500m near the tropopause. The domain top is at 20km with a Newtonian damping layer above 16km to absorb gravity waves. The damping layer does not impinge on the tropopause which is at 12km.

3.2. Experimental design

The experiments performed have two phases. In the first phase a state of radiative convective equilibrium (RCE) is established by running the model for a sufficiently long time with a constant imposed forcing. Thus, a three-dimensional RCE is used as the initial state for the second phase, in which the imposed surface forcing is time varying. In the time-varying phase, the forcing follows a continually repeated cycle. Experiments have been performed for various lengths of the forcing cycle, specifically for 1, 3, 6, 12, 18, 24 and 36hr. The experiments are designed to investigate convective memory at diurnal and sub-diurnal timescales for which variations in surface forcing may be important. Their design would not be appropriate for synoptic timescales, at which variability in forcing is

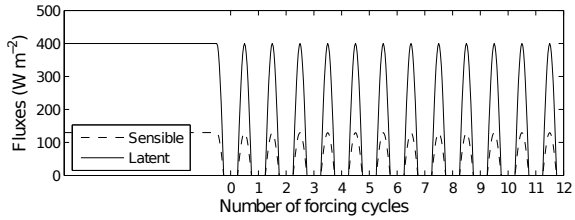

Figure 1. The figure shows the experimental setup for the surface forcing. During the first phase, constant surface fluxes of sensible (dashed line) and latent (solid line) heat flux are imposed. During the second phase, repeating cycles of time-varying surface fluxes are imposed. 11 successive forcing cycles are analysed, after the removal of some cycles for adjustment to the second phase. The number of cycles removed is given in Table 1.

usually associated with variability in large-scale dynamical ascent.

The forcing consists of a prescribed tropospheric cooling and prescribed surface fluxes of sensible and latent heat. We use the term radiative-convective equilibrium in a generic sense, with the tropospheric forcing being considered to represent the destabilization arising from processes acting in the absence of convective activity. Thus, it includes the effects of longwave cooling and large-scale ascent. The cooling is held constant in each phase of the experiments but the surface fluxes vary in time in the second phase.

The tropospheric cooling profile is similar to that used in various other idealized studies of RCE (e.g. Shutts and Gray 1999; Cohen and Craig 2006; Parodi and Emanuel 2009). Specifically, the cooling is uniform from the surface up to 400mb and decreases linearly with height until it vanishes at 140mb. No cooling is imposed above 140mb. The prescribed cooling rate in the first phase is 6.5Kd^{-1}, and this is reduced to 2.4Kd^{-1} for the second phase. These magnitudes of the cooling rate are chosen such that the combination of prescribed cooling and prescribed surface fluxes produces a balanced budget for the mass-weighted, vertically-integrated moist static energy. In the first phase of the experiments, the balance holds instantaneously at all times, whilst in the second phase the balance holds when the forcing is time-integrated over a forcing cycle. Whilst the magnitude of the cooling is large, recall that this term serves to account also for the atmospheric destabilisation that would be caused by vertical advection. Hence the function of this term is as a large-scale forcing term rather than a pure radiative term.

Figure 1 shows a schematic of the prescribed surface fluxes. The constant surface fluxes in the first phase are equal to the maximum fluxes in the second phase, the values being 130Wm^{-2} and 400Wm^{-2} for the sensible and latent heat fluxes respectively. Prescribing the surface fluxes means that we choose to consider these as strictly an aspect of the convective forcing rather than the convective response. This strategy is a departure from most RCE studies which typically specify a fixed sea surface temperature (SST) and allow the fluxes to adjust over time in order to achieve the moist static energy balance. The advantage in prescribing the fluxes for the aims of this study is that during the second phase the aspects of the system that are considered as forcing remain strictly repeatable on every cycle with no feedback to the forcing from any variability in the convective response. Thus, we maintain detailed control of the global moist static energy balance in a way that would not be possible with prescribed SST. Such control is important for the present purposes, since the experiments are run for a succession of cycles and we wish to ensure that the convective forcing is identical on every forcing cycle. Given that the imposed forcing is identical on every cycle, the convective response produced should also be identical on every cycle if equilibrium holds good at the forcing timescale of interest. Hence, any cycle-to-cycle variability in the convective response in these simulations provides a convenient and unambiguous measure of departures from equilibrium.

Prescribed surfaces fluxes have previously been used in simulations of the diurnal cycle over land. A suitable form for the time variation in the second phase has been chosen based on the EUROCS (European Cloud Systems Project) case study of Guichard *et al.* (2004) and specifically we have adopted the idealization of observed surface fluxes used by Stirling and Petch (2004), who also did not prescribe a mean wind. Thus, the fluxes vary as the positive part of a sine wave for half of the cycle, and are set to zero for the other half. Of course, the time variations are rescaled here such that they take place over the desired forcing timescale. For convenience, the initial profiles for the first phase of the experiments were also taken from this EUROCS case.

Davies (2008) compared RCE results obtained with prescribed surface fluxes to those obtained with prescribed surface properties that were chosen to produce the same domain-mean sensible and latent heat fluxes. There were very limited differences in the domain-mean characteristics of these simulations, and in a variety of cloud statistics. The main difference was a stronger tendency for clouds to clump together when using prescribed surface fluxes, which may be attributable to the more prominent cold pools.

4. Results

The results presented will focus on contrasting aspects of the simulated convection for different forcing timescales. Section 4.1 sets the scene with a comparison of timeseries of the convective mass flux. The process of adjustment to a time-varying forcing at the beginning of the second phase is the subject of Section 4.2, as this is a necessary preliminary to Section 4.3 which considers cycle-to-cycle variability. Finally, in Sections 4.4, 4.5 and 4.6 we explore which aspects of the simulated ensemble might carry some signature of memory, considering in turn the domain-mean fields, the self-organization of the cloud field, and the sub-domain variability. For brevity, it will be convenient henceforth to label the experiment with a forcing cycle of period 3hr as the "3hr simulation", and similarly for the other simulations.

4.1. Time evolution of convection for differing forcing timescales

Timeseries of the cloud-base mass flux are shown in Figure 2 for the second phase of each of the experiments. Also presented are composites of the cloud-base mass flux evolution over a forcing cycle. These are given in Figure 3, for the forcing periods of 36 and 3hr.

For the longest forcing timescales, 36 and 24hr in Figure 2(a) and 2(b) respectively, there is a strong convective response when the surface forcing is active but very little response while it is switched off. A spike in

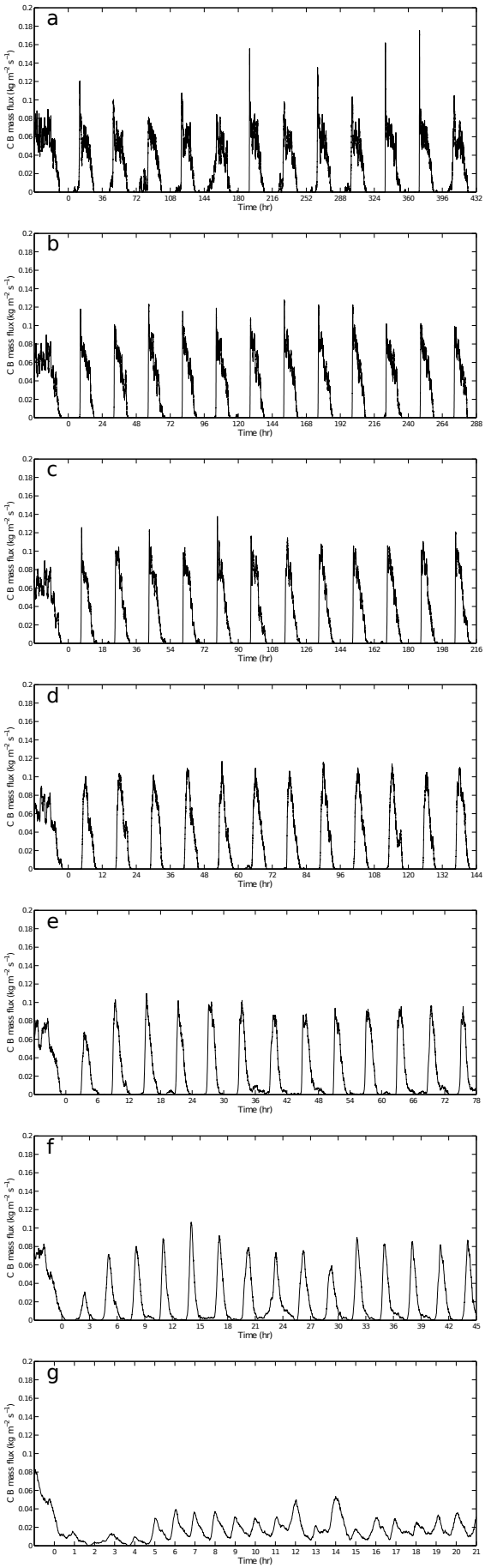

Figure 2. Timeseries of cloud-base mass flux for various periods of the forcing cyle: a) 36hr, b) 24hr, c) 18hr, d) 12hr, e) 6hr, f) 3hr and g) 1hr. Time zero corresponds to the start of the second phase of the experiments, as in Figure 1.

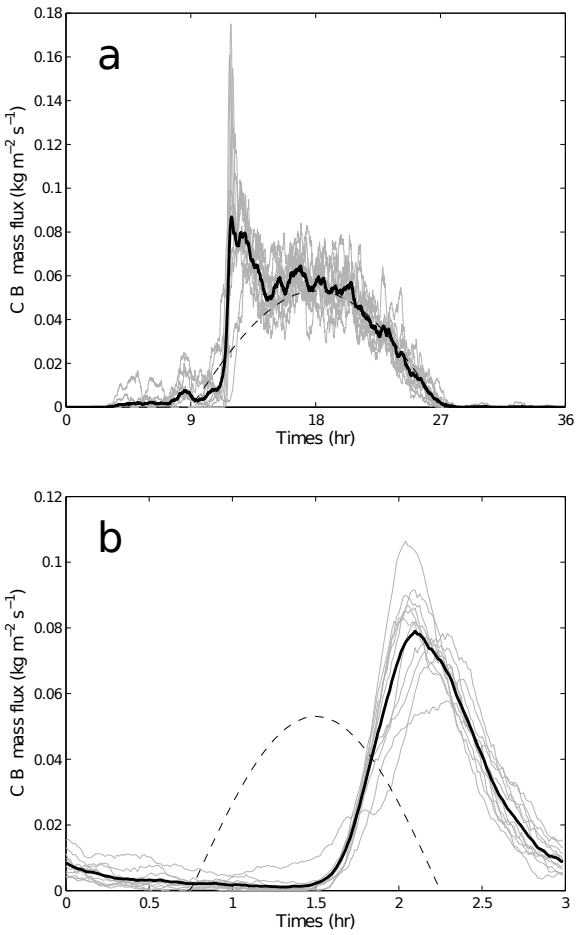

Figure 3. Time evolution of the cloud-base mass flux across a forcing cycle for forcing periods of: a) 36hr and b) 3hr. The heavy line is a composite of 11 successive forcing cycles following an initial adjustment at the start of the second phase of the experiments (see Section 4.2). The evolution within each of these forcing periods is shown in grey. Also plotted for reference is the time evolution of the prescribed surface flux forcing (dashed line), which has a peak value of $530\mathrm{Wm}^{-2}$.

activity occurs when convection is triggered on each cycle. At first sight, it may be tempting to interpret the spike as a purely artificial feature. As discussed in Section 3.1, fine resolution is required to represent the transition from shallow to deep convection in a diurnal cycle. A delayed onset of convection with an overshoot on triggering would not be unexpected at coarser resolution (e.g. Petch 2006). We performed some sensitivity tests looking at finer and coarser resolutions and whilst a finer resolution does reduce the spike somewhat, the onset of convection nonetheless remains strong and rapid. In particular, any uncertainties in the details of the triggering are not sufficient to affect the conclusions drawn from cycle-integrated metrics in Section 4.3. Moreover, investigation of cloud characteristics close to the time of onset showed that the clouds produced with a 1km grid length were not restricted to the grid scale, but had a clearly discernible range of sizes. Therefore, the strong mass flux at triggering in these simulations, and the absence of a distinct shallow convective phase, does appear to be a genuine feature of the experimental setup. The free troposphere remains close to neutral for moist convective ascent so that deep convection is triggered as soon as the boundary layer inversion is eroded. A discussion

of the initial profiles of temperature and moisture is given in Section 4.4.

An interesting feature to note in the 36hr simulation is that for some cycles (for example at around 72 and 144hr in Figure 2), non-zero cloud-base mass flux is produced shortly before the surface-flux forcing is switched on. During the comparatively long period for which the surface-flux forcing is switched off, instability may develop as a result of the tropospheric cooling alone. Such behaviour is not the focus of this study. For this reason, although the feature is infrequent and weak, there will not be great emphasis placed on analysis of the 36hr simulation.

For the longer forcing timescales, after the onset of convection, the cloud-base mass flux broadly follows the shape of the surface-flux forcing (e.g., Figure 3(a)). Moreover, the variation between cycles is small, so that the convection exhibits a consistent response to the forcing. Such behaviour indicates a predictable regime with the forcing timescale being long compared to the timescale of any memory effects (cf. Section 2).

For the shorter forcing timescales, the onset of convection on each cycle is more gradual and there are no spikes in the mass flux timeseries. A lag in the onset, relative to the start of the surface-flux forcing, is readily apparent. The time lag in absolute terms is dictated by the need to erode a boundary-layer inversion which develops while the surface fluxes are switched off. This lag time has rather little sensitivity to the forcing timescale, and so the lag relative to the forcing timescale becomes progressively more marked as the timescale decreases. For the forcing timescale of 3hr, the composite in Figure 3(b) shows that the cloud-base mass flux has its maximum as the surface-flux forcing switches off.

Also readily apparent from Figures 2(f) and 3(b) is the variability in the cloud-base mass flux from cycle to cycle in the 3hr simulation. As discussed previously such variability suggests that an element of memory may be playing a role in the simulation. The variability will be quantified in Section 4.3 and its physical origin will be discussed in Sections 4.4 to 4.6.

The shortest forcing timescale considered is 1hr. This is comparable with the time required to trigger convection in the other simulations, so a qualitative change in behaviour is anticipated. In this simulation an inversion does not develop while the surface-flux forcing is switched off and as a result convective activity is persistent throughout the forcing cycle (Figure 2(g)). Such behaviour seems to approach a regime where the memory timescale is long compared to the forcing timescale, so that the convection occurs at an almost-steady level with some moderate fluctuations.

Although the present discussion is based on timeseries of cloud-base mass flux, the characterisation of convective activity for different forcing timescales is not dependent on this choice of diagnostic. Similar behaviours can easily be identified using surface precipitation data for example. Precipitation first occurs around 30min after the onset of convection. This is consistent with expectations for microphysical processes to develop rainfall (e.g. Rogers and Yau 1989), and no dependence of such processes on the forcing timescale could be discerned.

4.2. Adjustment to the second phase of forcing

When the character of the forcing changes from the first to the second phase of the experiments (i.e., from a constant to a periodic forcing) there is an initial period of transient behaviour before the convective activity exhibits a more settled pattern. Such transients can be clearly seen during the first few forcing cycles in Figures 2(f) and (g) for example. We wish to remove the effects of such transients in order to study the cycle-to-cycle behaviour of the convection once it has adjusted to a periodic form of the forcing.

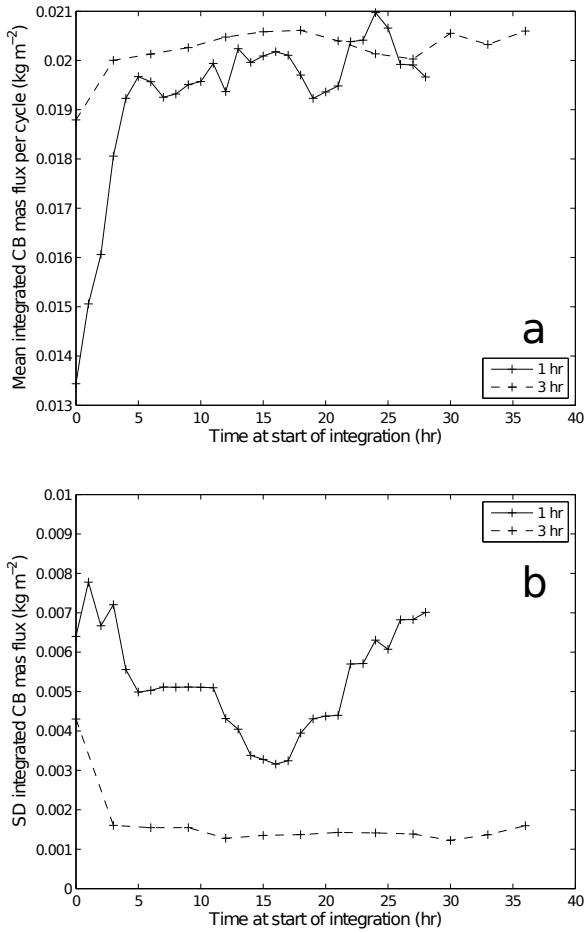

Figure 4. Effect of the time window used on the values of (a) $\overline{\langle M_b \rangle}$ and (b) $\sigma(\langle M_b \rangle)$. The calculations are made over 11 successive forcing cycles and the results plotted as a function of the time at the start of the sequence, for the simulations with forcing timescales of 3hr (dashed line) and 1hr (solid line). Time zero corresponds to the start of the second phase of the experiments, as in Figure 1.

A diagnostic of particular interest is the cloud-base mass flux time-averaged over a forcing cycle. Defining a single-cycle time-average by angled brackets, we denote this diagnostic by $\langle M_b \rangle$. The mean and standard deviation of the cycle-average over several successive cycles may then be written as $\overline{\langle M_b \rangle}$ and $\sigma(\langle M_b \rangle)$ respectively. Figure 4 shows these quantities for 11 successive cycles of the 3 and 1hr simulations, as a function of the first cycle that is included in the sequence. After a sufficient number of early cycles have been disregarded, $\overline{\langle M_b \rangle}$ tends to a value of $\approx 0.02 \mathrm{kgm}^{-2}$ for both forcing timescales, as indeed it does for the other forcings simulated. This represents simply the strength of convection required to balance the time-average magnitude of the prescribed forcing.

The first phase of the experiments has a stronger cloud-base mass flux than the second phase, the mean value

Table 1. Number of complete forcing cycles removed prior to timeseries analysis in order to account for adjustment to the time-varying forcing.

Forcing timescale (hr)	36	24	18	12	6	3	1
Number of cycles	1	1	1	1	2	4	10

being larger by a factor of around π in accordance with the mean strength of forcing. According to Figure 4(a) the time needed to suppress the previous level of convection and adjust to the time-varying forcing is ~ 5 to 7hr for both the 1hr and the 3hr simulations. A similar adjustment time is apparent for $\sigma(\langle M_b \rangle)$ (Figure 4(b)) in the 3hr simulation. However, in the 1hr simulation there are fluctuations in the timeseries that persist beyond 11 cycles such that $\sigma(\langle M_b \rangle)$ does not reach a steady value even after 27hr.

For longer values of the forcing timescale, the adjustment time becomes comparable to or less than the forcing timescale and so a suitable value for the adjustment time cannot be simply extracted from a visual inspection of the mass flux timeseries. We will assume that an adjustment of ~ 5 to 7hr still applies, and from all of the simulation data an initial period at the start of the second phase is removed from the timeseries before further analysis of the 11 following cycles is carried out (as for the composites in Figure 3 for instance). The adjustment period has been chosen to be not less than 10hr, rounded up to a whole number of forcing cycles. The number of forcing cycles removed for each simulation is listed in Table 1.

4.3. Characterising cycle-to-cycle variations

We now present results for $\overline{\langle M_b \rangle}$ and $\sigma(\langle M_b \rangle)$ as a function of the forcing timescale, with the adjustment period removed. Very similar values of $\overline{\langle M_b \rangle}$ occur regardless of the forcing timescale, as shown in Figure 5(a), this diagnostic being dictated primarily by the mean strength of the imposed forcing as noted above. Also demonstrated by this panel is the increased cycle-to-cycle variability for shorter values of forcing timescale. The sensitivity of $\sigma(\langle M_b \rangle)$ to the number of cycles considered has been tested for the 3 and 1hr timescales. For the 1hr case, the result is indeed somewhat sensitive to the number of cycles considered, but the main result of increased variability for shorter forcing timescales is robust.

For the longer forcing timescales, the mass flux integrated over a cycle varies very little from one cycle to the next, the convection is highly repetitive and there is no memory apparent within the system. For the shorter forcing timescales, however, the mass flux timeseries is less repetitive and the strength of the convective response differs from cycle-to-cycle, thereby indicating an element of memory. We have checked that the variability at these timescales exceeds that which would occur from an equivalent time-averaging of mass flux timeseries at RCE. For the shortest forcing timescale of 1hr, it is clear that the convection is not able to keep pace with the imposed forcing, and as a result the convection never dies out but rather oscillates about a mean response. Thus, the memory has become such a strong element in the system that the time-mean forcing is more important than its instantaneous value.

If the results above do indicate a role for memory within convective systems (as opposed to variations in $\sigma(\langle M_b \rangle)$ arising from sampling error for example), then one would expect to be able to find corroborating evidence that the convective activity during one forcing cycle affects the activity on a subsequent cycle or cycles. Figure 6 is a scatter plot of the cycle-integrated cloud-base mass flux $\langle M_b \rangle$ on one forcing cycle against that on the next cycle. It can be seen that there is a discernible relationship between the convective activity on successive cycles with correlations of -0.51, -0.39 and -0.52 for the forcing timescales 12, 6 and 3hr respectively. For the 1hr forcing timescale (not shown), no such relationship is apparent, just as would be expected for this diagnostic if the memory timescale becomes long relative to the forcing timescale.

Figure 5(b) illustrates that these results are not dependent on the choice of convective diagnostic, with the same characteristics apparent when considering surface precipitation.

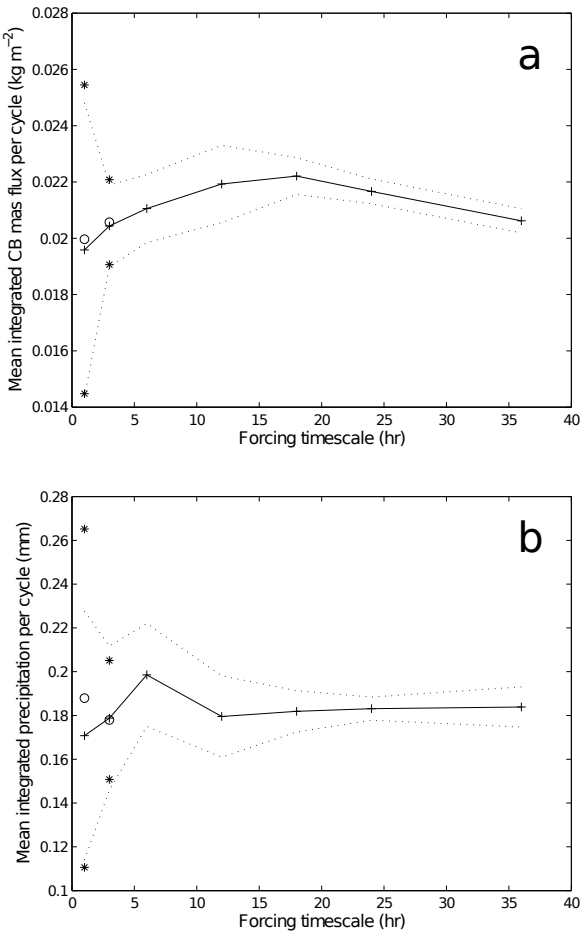

Figure 5. a) The cycle-mean cloud-base mass flux, and its standard deviation, as evaluated from 11 successive forcing cycles with the adjustment period removed: $\overline{\langle M_b \rangle}$ (solid line with crosses) and $\overline{\langle M_b \rangle} \pm \sigma(\langle M_b \rangle)$ (dotted lines). b) As in a) but for the surface precipitation $\langle I_{ppt} \rangle$. The additional symbols for the forcing periods of 3 and 1hr show results from evaluations with more cycles being included: 16 and 29 successive cycles respectively, again with adjustment period having been removed. The open circles are for the mean values and the asterisks indicate the mean plus or minus one standard deviation.

4.4. Role of the mean state

It has been found that for short forcing timescales there is some feedback between the cycle-integrated convection on

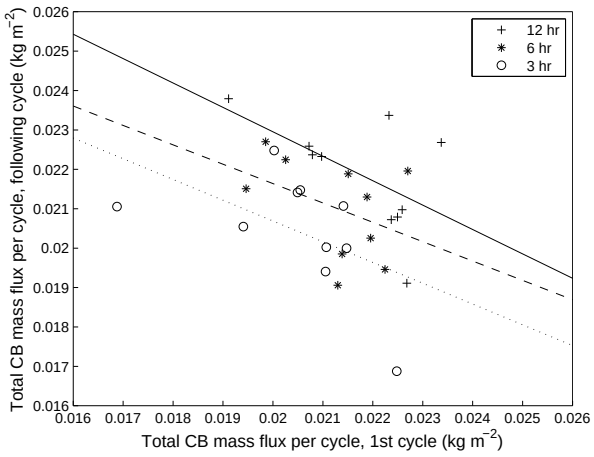

Figure 6. Scatter plot of cycle-integrated cloud-base mass flux on one forcing cycle against that on the next. Results for forcing timescales of 12 (crosses), 6 (asterisks) and 3hr (open circles). Also plotted are lines of least-squares linear regression for each of the forcing timescales, 12 (solid), 6 (dashed) and 3hr (dotted).

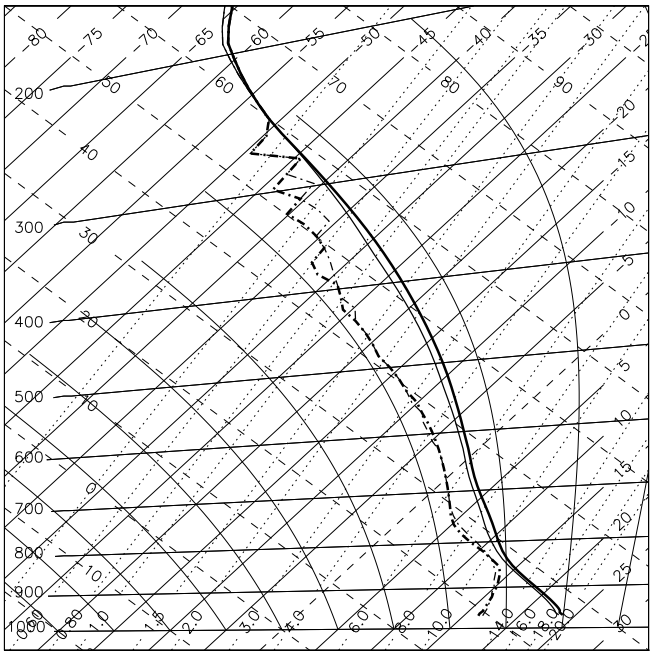

Figure 7. Tephigram showing domain-mean vertical profiles at the start of the forcing cycle for the 24 and 3hr simulations. The profiles have been composited from 11 successive cycles, with the adjustment period removed. The 24hr simulation is shown as solid lines and the 3hr simulation as thicker lines.

successive cycles, which is sufficient to alter the qualitative nature of convective timeseries. We now consider whether such cycle-to-cycle memory might be carried by variations in the domain-mean state at the start of each forcing cycle. A simple explanation for the above results could be that the convective activity on a previous cycle modifies the domain-scale environment in such a way as to promote more (or less) intense convection during the following cycle.

The start of a forcing cycle is defined as being the time when the imposed surface heat flux becomes positive. Domain-mean states at this time are shown on a tephigram in Figure 7, composited over 11 successive cycles, for forcing timescales of 24 and 3hr. The 24hr simulation is chosen as an example of a system not affected by memory and the 3hr simulation as an example in which memory appears to be important. The initial profiles are similar in these simulations, although the 3hr simulation is slightly warmer at all levels. The 3hr simulation shows a more well-mixed moisture profile near the surface, probably reflecting the fact that there is still some convective activity in the domain, even as a new forcing cycle begins.

To determine how variable the initial profiles are from cycle to cycle, the domain-mean relative humidity is shown in Figure 8(a) as box plots at several levels. As a result of the cooler atmosphere, relative humidity is larger at all levels in the 24hr simulation compared to the 3hr simulation, particularly at higher levels. There is greater variability in the relative humidity profiles in the 3hr simulation. Figure 8(b) shows that at the start of each forcing cycle in the 24hr simulation there is no upward or downward domain-mean motion: all previous convection has decayed. However, the 3hr simulation does show some domain-mean vertical velocity of up to ~ 2 mms^{-1} at the start of the forcing cycle, indicating that residual activity from convection on the previous cycle is still present.

The increased variability in the initial state of the 3hr simulation is consistent with the idea that a signature of memory might reside in the domain-mean initial state. We can test the idea by looking for any differences in that state depending on whether it proceeds stronger or weaker convection within the following cycle. If true, that would imply that the convection integrated over the cycle has some degree of predictability in a parmeterization based on the mean state and the large-scale forcing, even if it is not in balance with the forcing. A sequence of 20 cycles is partitioned into six strong, eight medium and six weak cycles, according to the cycle-averaged cloud-base mass flux. The initial profiles of relative humidity for the strong and weak cycles are shown in Figure 9 at several levels. The relative humidity tends to be slightly lower in the boundary layer and slightly larger in the free troposphere in the initial states preceeding stronger convective activity. The lower boundary layer values arise from a combination of lower values of water vapour mixing ratio and higher temperatures, whilst the larger relative humidity above arises from lower temperatures with very similar values of water vapour. This suggests that the domain-mean atmosphere does tend to be slightly more conducive for convection on average ahead of a cycle of stronger activity but such cycles would not be distinguishable from the mean convective response at the start of the forcing cycle. However, the most important point to emerge from Figure 9 is that there is how little difference occurs between the partitions when judged relative to the variability within each partition. We conclude that the mechanisms which cause one forcing cycle to have more or less activity than another are not encompassed by the domain-mean initial state. The implication for parameterization is that an additional variable characterising sub-grid scales would be required to capture the memory effects found in these simulations.

4.5. Cloud statistics and the time evolution of self-organization

The results of Sections 4.1 and 4.3 showed that the simulated convection has an element of memory if it is rapidly forced. However, such memory does not appear to be carried by the domain-mean state at the start of

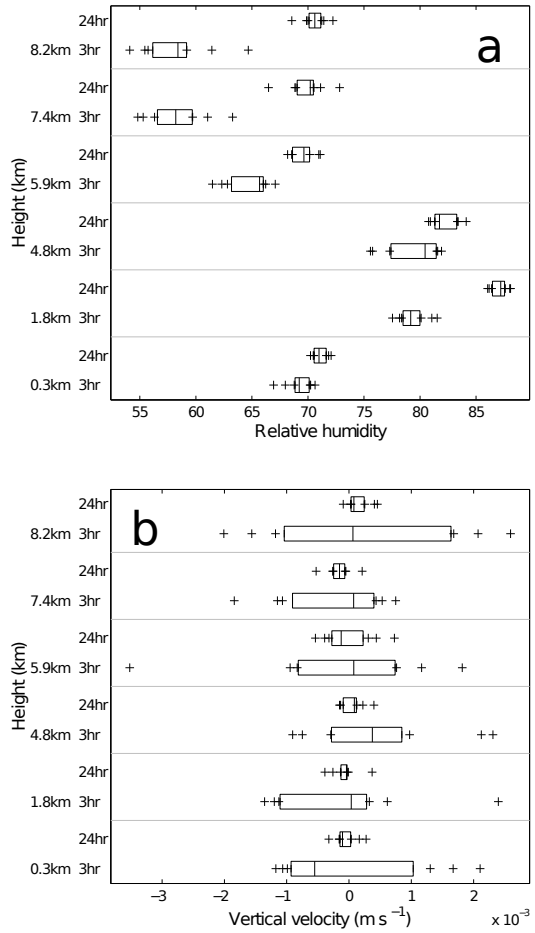

Figure 8. Domain-mean vertical profiles at the start of the forcing cycle for (a) relative humidity and (b) vertical velocity are shown as box plots at several levels for the 24hr and 3hr simulation. The profiles have been composited from 11 successive cycles, with the adjustment period removed. The width of the box shows the interquartile range from the 25th to 75th percentile, the mean is shown by a vertical line and all points outside this range are shown as plusses.

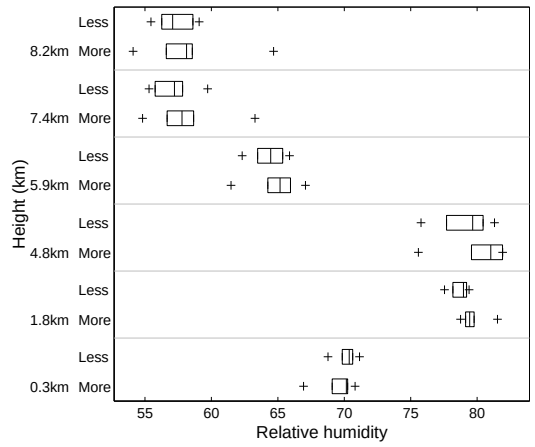

Figure 9. Domain-mean vertical profiles of relative humidity at the start of the forcing cycle at several levels for the 3hr simulation. A sequence of 20 cycles from the 3hr simulation is considered, following the adjustment period. The cycles are partitioned into six with strong convective activity, eight with medium activity and six with weak activity, the activity being measured by the cycle-averaged cloud-base mass flux. The profiles are shown as box plots for the cycles with strong subsequent convection, labelled 'more', and for the cycles with weak subsequent convection, labelled 'less'. The format of the box plot is as in Figure 8.

each cycle (Section 4.4). In the present subsection, we turn our attention to the time evolution of the cloud structure. In particular, the role of clouds in modifying horizontal thermodynamic structure will be discussed. The spatial distribution of the convective clouds and the local aspects of their warming and moistening of the atmosphere produce inhomogeneities in the thermodynamic fields. Such horizontal variability may persist into a subsequent cycle and influence the triggering of future clouds.

Before presenting the cloud statistics, we briefly comment on two sub-domain features that do not appear to be responsible for carrying memory in these experiments. We investigated whether cold pools or anvil clouds might provide a suitable mechanism. No systematic differences were found in the strength of the cold pools between simulations, or between cycles of the 3hr simulation with strong and weak convective activity. The simulations do produce anvil cloud above deep convection but this is short-lived. It does not persist from cycle to cycle and hence does not play a role in modifying subsequent convection. It should be recalled, however, that the experimental design deliberately excludes cloud-radiative and surface-flux interactions which would impact on anvil cloud and cold pools, so we do not rule out the possibility that these features may provide memory mechanisms in other situations, particularly if such interactions are important.

Statistics of convective clouds in the 3 and 24hr simulations are shown in Figure 10. A convective cloud is defined here as a group of one or more connected grid-points that are both buoyant and upward-moving, and with cloud water in excess of 1×10^{-5} kg kg^{-1}. Similar definitions have been used elsewhere (e.g. Khairoutdinov and Randall 2006). The total convective mass flux is the product of the number of clouds and the mean mass flux per cloud. These two components are shown as functions of time and height in Figure 10. In the 24hr simulation, the clouds very rapidly become deep once triggered. The mass flux carried by these clouds is relatively weak in comparison with the clouds that develop later in the cycle, but they are nonetheless sufficiently numerous to cause a 'spike' in the cloud base mass flux (Section 4.1). Thus, the spike arises because the triggering occurs almost simultaneously at many locations within an atmosphere that is close to moist adiabatic (Figure 8). By contrast, the 3hr simulation shows a more gradual development in height as the clouds deepen through a slightly warmer troposphere that has lower relative humdity. The increase in total mass flux is dominated by an increase in cloud number rather than strength. Clouds do become somewhat weaker during the decay of convective activity, for both 24 and 3hr simulations, but a reduction in the number of clouds oer time is the main factor in the reduction of total mass flux. Aside from the spike feature, there are typically fewer, stronger clouds in the 24hr.

The spatial structure of the clouds is shown in terms of the cloud-spacing distributions in Figure 11. For each convective cloud (defined as above), the distances to all other clouds in the domain are computed, the distance being that between the mid-points of the clouds in question. The cumulative distribution of all pairwise inter-cloud spacings is then formed and is normalised by the cumulative distribution that would occur for the same number of clouds distributed randomly in space. Values larger than unity indicate a tendency for clouds to clump together at a particular scale, whereas values less than unity indicate a

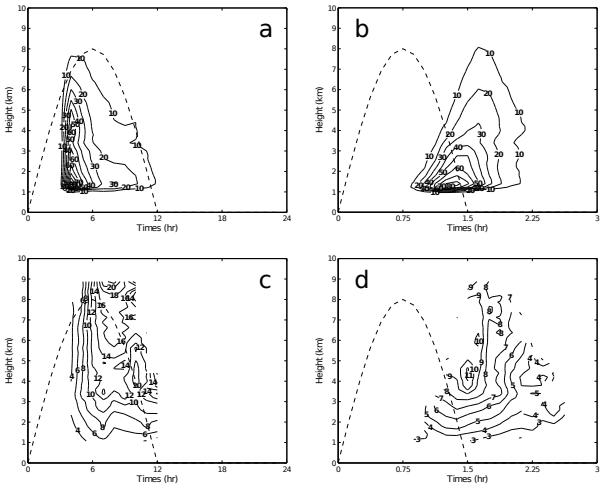

Figure 10. Time evolution of domain-mean cloud properties for the 24hr simulation, in (a) and (c), and for the 3hr simulation, in (b) and (d). The properties are evaluated as averages over 11 successive cycles, with the adjustment period removed. The mean number of clouds in the domain is shown in (a) and (b) and the mean mass flux per cloud in (c) and (d), the units of mass flux being $\mathrm{kgm^{-2}s^{-1}}$. Also plotted for reference is the time evolution of the prescribed surface flux forcing (dashed line), which has a peak value of $530\mathrm{Wm^{-2}}$.

Table 2. Definition of key times within the forcing cycle for 24 and 3hr simulations. The key times are defined so as to provide comparable points within the two cycles, which necessitates the use of different definitions for the convective minimum.

Name	Definition
Pre-forcing	1hr before the surface fluxes are switched on
Triggering	Time when cloud-base mass flux first reaches 50% of its peak value
Convective maximum	Maximum of cloud-base mass flux excluding any spike at triggering
End of convection	Time when the surface fluxes are switched off
Convective minimum (24hr simulation)	Midpoint of the time during which the surface fluxes are switched off
Convective minimum (3hr simulation)	Minimum of cloud-base mass flux

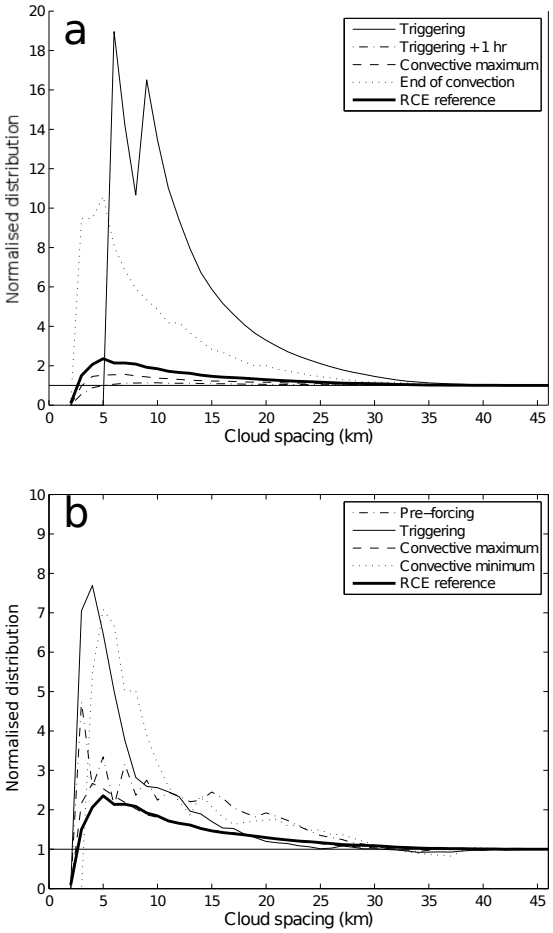

Figure 11. Normalized cloud-spacing distributions computed at a height of 3km for key times during the forcing cycle. Panel (a) shows results for the 24hr simulation, at the times of triggering (solid), 1hr after triggering (dash-dotted), convective maximum (short dashed) and at the end of convection (dotted). Panel (b) shows results for the 3hr simulation, at the times of pre-forcing (long-dashed), triggering (solid), convective maximum (short dashed) and convective minimum (dotted). The times are defined in Table 2. Also plotted is the distribution obtained at RCE during the first phase of the experiments. Note the differing y-axis.

tendency for repulsion. Figure 11 shows the cloud-spacing distributions at key times within the forcing cycles, for the simulations with forcing timescales of 24 and 3hr. The key times are defined in Table 2.

For reference, we note that limited self-organization of the cloud field occurs at RCE. Figure 11 also shows the RCE distribution from the first phase of the experiments, which indicates a tendency for clouds to clump together at scales of up to ≈ 20km. A similar clumping tendency can also be seen in the RCE cloud-spacing distributions plotted in Figure 6a of Cohen and Craig (2006), provided that the forcing strength is not too large.

At the time of triggering the first convective clouds to form are strongly clumped. For the 3hr forcing timescale, the preferred cloud spacings are $\approx 3-10$km, while for the 24hr timescale the organization is even more prominent and occurs over a larger range of cloud spacings, $\approx 5-25$km. Recall from Section 4.1 that deep convection is produced as soon as a boundary-layer inversion is eroded. A possible explanation for the organization in the cloud field at this time is that there are areas which are somewhat more favourable for the erosion and triggering, so that the size of those areas dictates the scale of preferred cloud spacings. Another possibility is that the triggering of the very first convective cells rapidly modifies the neighbouring environment, for example by producing gravity waves which may preferentially assist initiation in the immediate vicinity of the parent cell (e.g. Marsham and Parker 2006). Regardless of the detailed mechanism, it is notable that the organization occurring at triggering decays rapidly in the 24hr simulation. In that case the cloud-spacing distribution is close to being random 1hr later at which time there are fewer clouds in the domain than at triggering, but the individual clouds are stronger.

In the 24hr simulation, as the convection evolves further towards its "maximum" activity, the cloud-spacing distribution remains close to being random. There is some indication of short-range clumping, but this is weaker than

at RCE. By comparison, in the 3hr simulation there is a montonic decay in the strength of the organization, such that by the time of convective maximum, the cloud-spacing distribution is similar to that at RCE.

For both of the forcing timescales, organization becomes more apparent within the cloud-spacing distribution as the convection decays. In the 24hr simulation, there is a period during which convective activity is extinguished (Figure 2(b)) and no convective clouds are diagnosed within the domain. Of course, it is then no longer possible to assess spatial inhomogeneities with the cloud spacing diagnostic, but Figure 11(a) demonstrates that there is pronounced clumping present when the surface fluxes are switched off. In the 3hr simulation, however, there remain sufficient clouds in the domain to determine the spacing distribution throughout the forcing cycle. The convection becomes increasingly organized as it decays, with the spacing distribution at convective minimum being similar to that at triggering, albeit displaced slightly upscale. Thus, when convection triggers on the next cycle it does so in a way that is consistent with the pre-existing scale of organization in the domain.

The picture emerging from the above analysis for the 24hr simulation is that convection is first initiated in clumps but that shortly afterwards the clouds are located almost randomly throughout the domain. Organization of the cloud field then increases over time, rather slowly while the convection is developing and more rapidly during decay. For the 3hr forcing timescale the pattern is less pronounced, with initial clumping reducing as convection increases to its maximum, and increasing as the convection decays. The organization in the cloud field clearly persists from one 3hr cycle to the next, which we propose may provide a means for transmitting a memory of the convection that occurred on the previous cycle. We now investigate this possibility further, and also explore whether other aspects of spatial structure might persist from cycle-to-cycle with a forcing timescale of 24hr.

In order to do so we have studied the evolution through a forcing cycle of the horizontal Fourier decomposition of various thermodynamic fields. Power spectra are shown in Figure 12 for the relative humidity at 3km. Since we are interested in the evolution of scales at which there is non-trivial structure in the cloud spacings, it is convenient to normalize the spectra such that the integral over wavenumber is unity. A similar picture emerges from a consideration of the evolution of spectra at other heights within the cloud layer, and for other thermodynamic fields, including both potential temperature and water vapour mixing ratio (Davies 2008).

Figure 12 focusses on two important times in the forcing cycle: when convection is at its maximum, and a little before triggering (taken to be the time of pre-forcing for the 24hr simulation and the time of convective minimum for the 3hr simulation). In the 24hr simulation, before the convection triggers the thermodynamic fields are essentially large-scale, with very little power below a wavelength of 20km. When the convection triggers power develops at very short wavelengths, characteristic of typical cloud sizes, but by the time of convective maximum the normalized power becomes more apparent at moderate wavelengths, of $\approx 5-20$km. As the convection starts to decay the normalized power is then reduced at both short and moderate wavelengths. Completing the cycle, after the surface forcing has been switched off spatial structure decays on all wavelengths, with the shift towards longer wavelengths continuing so that the relative humidity again becomes a predominantly large-scale field.

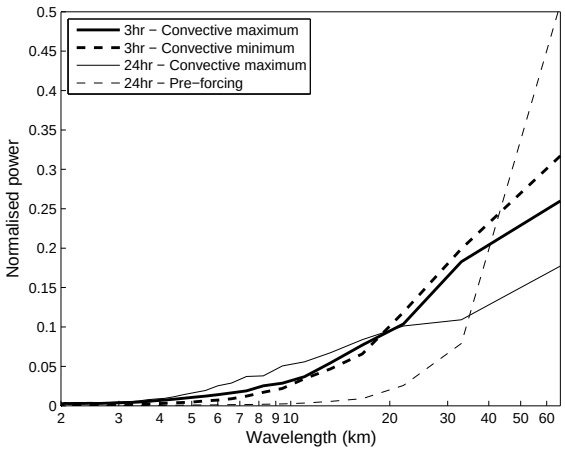

Figure 12. Normalized power spectra of the horizontal field of relative humidity at a height of 3km, for forcing timescales of 24hr (thin lines) and 3hr (thick lines). For each timescale the spectrum is shown for two key times within the forcing cycle, as defined in Table 2. For the 24hr simulation the times are convective maximum (thin solid) and pre-forcing (thin dashed); for the 3hr simulation the times are convective maximum (thick solid) and convective minimum (thick dashed).

By comparison, in the 3hr simulation the normalized spectra of thermodynamic variables undergo rather little temporal development through the forcing cycle. When convection is at its maximum, power is somewhat enhanced at small scales (more so for potential temperature; not shown), but this change is relatively modest. It should be stressed that the largest values of normalized power at moderate wavelengths occur for the 24hr simulation at convective maximum, and in this sense the longer forcing timescale produces stronger spatial organization in the thermodynamic fields at such scales. This might have been anticipated given that the same simulation has the stronger spatial organization in the cloud field at triggering, as discussed above. However, the moderate-scale organization in the thermodynamic fields is much more persistent in the 3hr simulation whereas in the 24hr case this decays strongly during the absence of convective activity.

4.6. Role of cloud-related small-scale structures

The previous subsection shows that, even in the absence of some imposed organizational mechanism such as wind shear or rotation, nonetheless the simulated convection does develop some self-organized structure. As the convection decays, spatial inhomogeneity remains in the thermodynamic fields. In the 24hr simulation such structures have almost vanished by the start of the next forcing cycle, but in the 3hr simulation such structure persists through the complete cycle and may influence the scale on which convection organizes on the subsequent cycle. Section 4.4 shows that the domain-mean relative humidity at the start of the forcing cycle is not substantially different between those cycles which subsequently have more or less convection, so that the mean state cannot be sufficient to account for memory effects. However, the persistence of spatial inhomogeneity in the 3hr simulation

raises the possibility that this may carry an element of memory. Here we investigate that possibility further by considering whether thermodynamic inhomogeneity induced by previous clouds might modify subsequent convection.

Figure 13(a) shows the domain-mean cloud base mass flux in the 3hr simulation, composited over each of the partitions of strong, weak and moderate convective cycles. The cycles with the strongest time-integrated convection achieve this through a stronger peak mass flux, whilst the cycles with the weakest time-integrated activity are characterised by a more rapid decay in convective activity. Figures 13(b) and (c) decompose the mass flux differences between the strong and weak cycles into the differences in cloud number and mean mass flux per cloud, respectively. The stronger peak of total mass flux is dominated by increased cloud number on the relevant cycles, whilst the more rapid decay on weaker cycles is mainly associated with a reduction in the strength of each cloud at this time. Further analysis (not shown) reveals that the reduced mass flux per cloud at later times on the weak cycles arises primarily from a reduction in in-cloud vertical velocities rather than any reduction in the cloud size. Thus, the strong cycles are characterised by triggering at more locations, whereas weak cycles are characterised by clouds developing within a more hostile local environment later in the cycle.

We now wish to establish whether spatial inhomogeneity at the start of the forcing cycle is related to the convective clouds that then develop. In order to do so, we first identify the horizontal location of the clouds at convective maximum. In practice this is done by taking five snapshots within a period of 0.5hr centered on the convective maximum and testing for locations where the convective cloud definition is satisfied on any vertical level at least three times. The relative humidity that was present at the start of the forcing cycle, averaged over the locations that later contain cloud, is shown in Figure 14. The results are partitioned into the cycles of strong and weak convective activity, and are constructed as differences with respect to the domain-mean relative humidity at that time. Use of the difference from the domain-mean is convenient in order to focus attention on spatial inhomogeneity, given that Figure 9 shows that the strong cycles are associated with higher domain-mean relative humidity.

Locations that will later contain clouds tend to have lower relative humidity than the domain-mean near the surface and higher values in the troposphere, particularly the lower troposphere. The anomalous relative humidity is larger for the partition with strong subsequent convection, most notably at 780mb (~ 1.8km) where there is little overlap between the distributions. This difference in relative humidity arises mainly from larger values of water mixing ratio, with some contribution from slightly lower temperatures (not shown). The result is complementary with the study of Stirling and Petch (2004) who stressed the importance of lower-tropospheric spatial variability in relative humidity for the initiation. Another feature of Figure 14 is the greater variability in the anomalous relative humidity preceeding cycles of weak convection. Thus, on cycles of strong convection, more clouds are triggered and are more closley tied to locations with anomalous relative humidity, whereas on cycles of weak convection the local humidity environment is a less important aspect of the triggering. The point that the local environment may be less favourable may in turn be related to the weaker mass flux per cloud later in the cycle (Figure 13(c)).

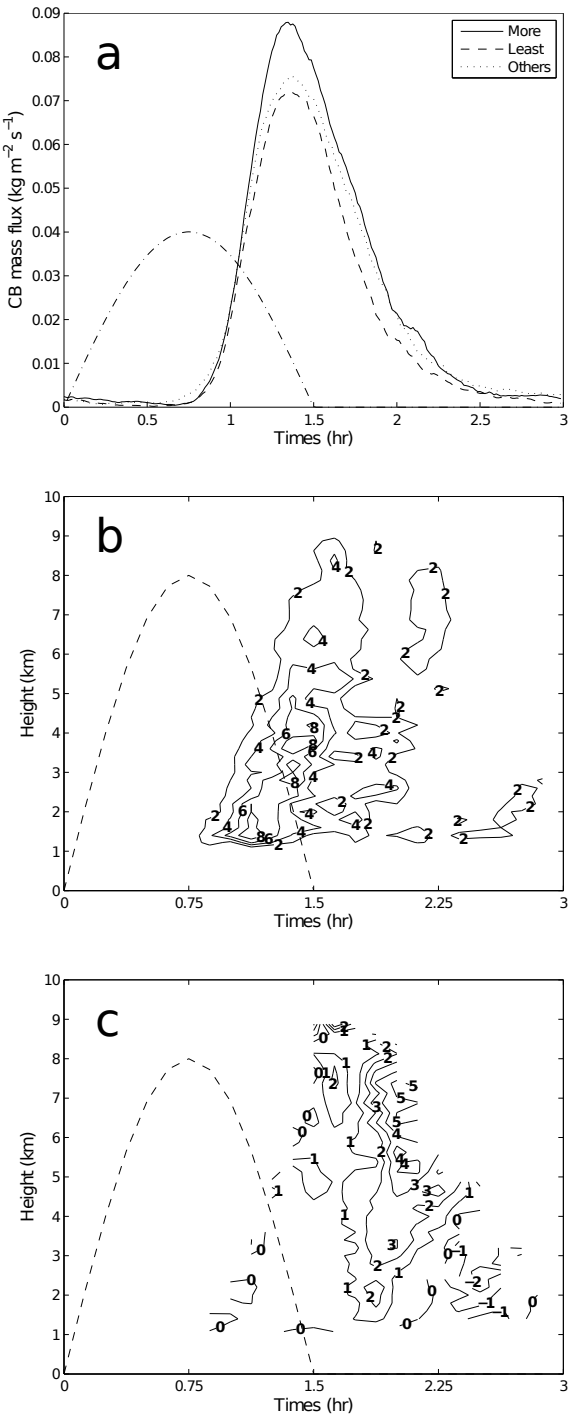

Figure 13. (a) Time evolution of the cloud-base mass flux across a forcing cycle for the 3hr simulation, composited within partitions that are defined by the cycle-integrated convection (Section 4.4). The partitions are for cycles with strong convection, labelled 'more', for cycles with weak convection, labelled 'less', and for cycles with moderate convection, labelled 'others'. Panels (b) and (c) show differences in domain-mean cloud properties between the partitions with strong and weak convection. Differences in cloud number are shown in (b) and differences in mean mass flux per cloud in (c). The units used for mass flux are kgm^{-2}s^{-1}. Also plotted for reference on all panels is the time evolution of the prescribed surface flux forcing (dashed line), which has a peak value of 530Wm^{-2}.

These interpretations are confirmed by Figure 15(a), which shows more detail of the horizontal distribution of

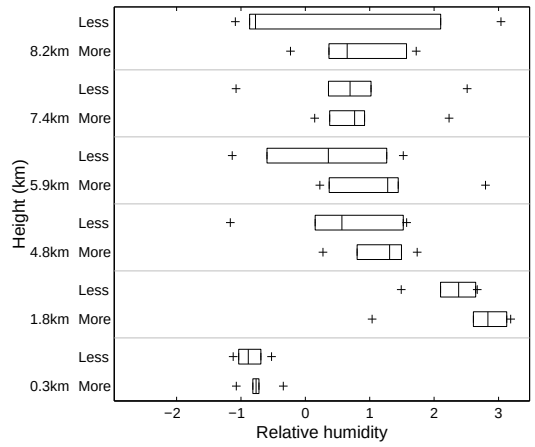

Figure 14. Profiles of anomalous relative humidity at the start of the forcing cycle for locations that will contain convective cloud during the subsequent forcing cycle. The method of identifying such locations is explained in the main text. The profiles are shown as box plots for the cycles with strong subsequent convection, labelled 'more', and for the cycles with weak subsequent convection, labelled 'less'. The format of the box plot is as in Figure 8.

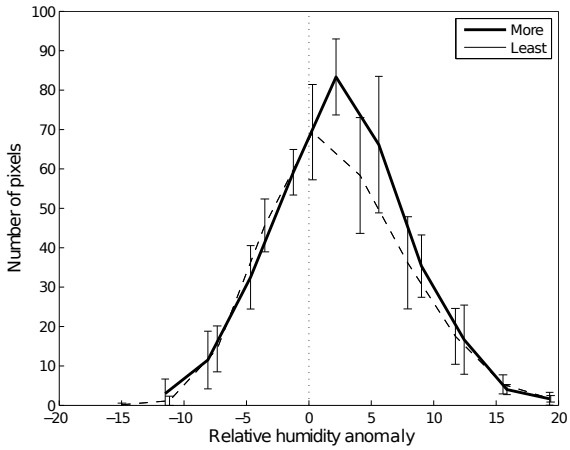

Figure 15. Distributions of the anomalous relative humidity at 780mb ($\sim$ 1.8km), constructed at the start of the forcing cycle from the values at all locations that will contain convective cloud in the following cycle. The method of identifying such locations is explained in the main text. The distributions are shown for cycles with strong subsequent convection (solid line, labelled 'more'), and for cycles with weak subsequent convection (dashed line, labelled 'less'). The distributions were calculated for 10 bins of equal width, with bars indicating one standard deviation.

anomalous relative humidity at 780mb, and compares the distributions that preceed the strong and weak cycles. (Note that there are more points included in the distribution for strong cycles, as a simple consequence of there being more clouds on those cycles.) The bias toward positive anomalies of relative humidity is readily apparent, as is the shift in the distribution to the right for those cycles that have strong convective activity. Both points emphasize the role of spatial inhomogeneity. Inspection of equivalent plots produced for other heights confirms that it is the inhomogeneity in the lower troposphere that is most important, particularly that around and just above cloud base.

Figure 16 presents a series of snapshots of the water vapour and cloud fields which summarise the evolution of spatial structure through a forcing cycle. For the longer forcing timescale of 24hr (above), the water vapour field at convective maximum convection exhibits prominent structures over a wide range of scales, with moist patches within and around the clouds. Such patches are dissipated somewhat as convection decays, and more strongly during its absence, to leave a weakly-varying, large-scale field just before triggering on the next cycle. When the convection does trigger it produces small clouds in both the moister and drier parts of the domain. For the shorter forcing timescale of 3hr, shorter scales of spatial variability are similarly apparent in the water vapour field at convective maximum. The key difference, however, is that there is much less time for such structure to decay and so shorter scales remain apparent when convection is triggered on the next cycle. Moreover, when that triggering occurs, the moisture variability is sufficiently strong that the new clouds are formed predominantly in the more moist regions of the domain. The more clouds that are triggered, and the more closely those clouds are related to the moisture anomalies, the stronger the convection will be on the subsequent cycle.

5. Conclusions

Many studies of equilibrium deep convection have been performed with cloud-system resolving models. In such studies, typically the forcing for convection is externally prescribed and held fixed in time, and the simulations are run for a sufficiently long time to obtain a quasi-steady convective state for detailed analysis. This approach has certainly had some success in explaining important sensitivities of convective ensembles and thereby developing parameterization for large-scale models. However, it is clear that treating the forcing as fixed in time and externally prescribed constitutes a very strong idealization of the real atmosphere. In recent years more attention has been given to considering cases more closely resembling a real convective atmosphere. One example is the development of methods for interactive forcings that respond to the simulated convection (e.g. Sobel and Bretherton 2000; Raymond and Zeng 2005; Kuang 2008; Daleu *et al.* 2012). The investigation here is complementary in the sense that it does prescribe the forcing, but that the forcing varies systematically in time. In particular, we consider a range of rapidly-varying forcing timescales in order to study how and under what circumstances convective ensembles exhibit departures from equilibrium. An important feature of the experimental design is the close control of the moist static energy budget, which is achieved through the specification of the vertical cooling profile and of the surface fluxes. This means that the imposed destabilization of the atmosphere is repeated on each forcing cycle, so that cycle-to-cycle differences in the convection provide a direct measure of departures from equilibrium on the imposed timescale.

The study presented here is based on a highly-idealized set of experiments, and clearly the simulated variability should only be associated with the explicitly simulated processes and the prescribed timescales. Other processes, such as radiative interactions and mesoscale variability, may be important for some real-world situations but have been deliberately excluded here in order to ensure a clean focus on factors that are intrinsic to the dynamics of (nearly) scattered convection and some directly-related small-scale processes.

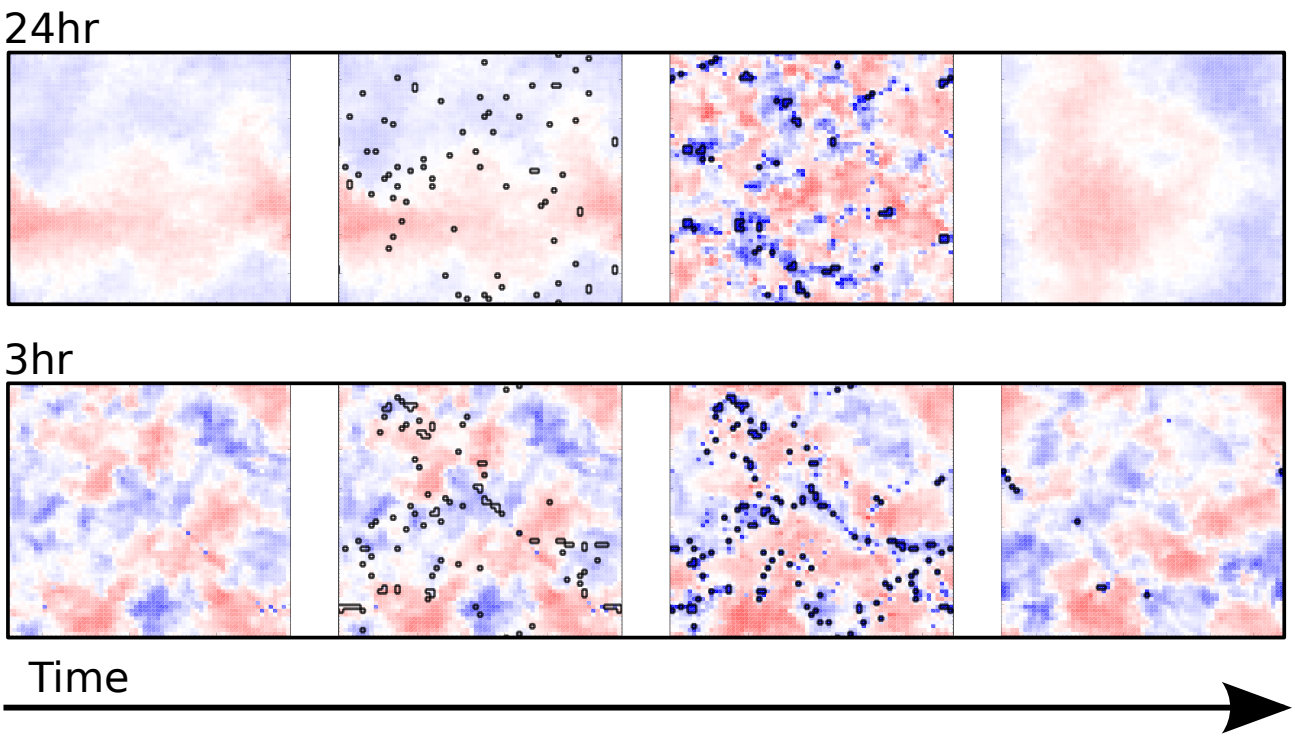

Figure 16. Snapshots illustrating the time evolution of the water vapour mixing ratio and cloud field at a height of 1.8km, in the 24hr (top panels) and 3hr (bottom panels) simulations. The times used are as defined in Table 2 with the four panels showing snapshots at (from left to right): pre-forcing/convective minimum (24hr/3hr simulation), pre-forcing/convective minimum (24hr/3hr simulation) moisture field with the cloud location at triggering superimposed, convective maximum and pre-forcing/convective minimum (24hr/3hr simulation) on the next cycle. The colours show water vapour anomalies in the range $\pm 2 \mathrm{gkg}^{-1}$ with blue colours indicating moist areas and red colours indicating dry areas. Black outlines show the location of convective clouds, diagnosed according to the definition stated in the main text.

In considering departures from equilibrium, it is convenient to distinguish between the instantaneous convective activity and the activity averaged on the timescale of the forcing: in other words, between the phase and the amplitude of the convection. The finite time required to erode an inversion (or perhaps in other circumstances to transition from shallow to deep convection) introduces a phase lag between convection and its forcing. The lag may be dependent on the variable used to measure convective activity (for example, the formation of precipitation lags somewhat further behind the forcing than the cloud-base mass flux) but the processes producing such lags are essentially internal to the dynamics and microphysics of convection.

For a forcing timescale of the order of a diurnal cycle or longer, the cycle-integrated amplitude of convective activity was found to be repeatable from one cycle to the next. The present experiments are a highly idealized set designed to study the dependence of convection on the forcing timescale, rather than to study a fully realistic diurnal cycle per se. Despite all the caveats that implies, it is nonetheless interesting to note that the diurnal cycle is not necessarily an out of equilibrium problem, at least in the limited sense discussed here of an equilibrium defined in terms of the cycle-integrated amplitude. This result differs from that of Jones and Randall (2009) equilibrium was not achieved over an equivalent area even for forcing timescales of 30hr. In their study convection must organise on large scales to achieve equilibrium whereas in this study convection develops locally and self-organises more rapidly.

One can imagine that if the forcing varies sufficiently quickly then variations in the forcing will scarcely be felt by the convection at all. For example, once a single ostensibly–deep cloud has been initiated, any rapid fluctuations in its environment are likely to lead to small perturbations rather than profound deviations in its development. The experiments performed here suggest that such a situation is approached when the forcing timescale is 1hr, comparable with convective cloud lifetimes. The finite cloud lifetime acts as a smoother for very rapid forcings, so that forcing variations produce only a modulation of a steady convective response.

For intermediate timescales of 3, 6 and 12hr we find systematic departures from equilibrium in both the phase and amplitude of the convection. Variability is found in the cycle-integrated convection, with departures from the equilibrium level of activity being negatively correlated between one cycle and the next. These points are consistent with the notion that the convective system has an element of memory, similarly to the analytic model proposed by Davies *et al.* (2009). A comparison of the domain-mean thermodynamic conditions prior to the onset of each cycle of convection shows that very similar conditions occur prior to cycles that are stronger and weaker than the average. This suggests that the memory is not predominantly carried by the domain-mean profiles and so a parameterization that is based only on the mean state will not be capable of predicting the cycle-to-cycle variations, other than in a statistical sense.

We propose that a more important mechanism for carrying a memory of previous convection from one cycle to the next occurs through the persistence of spatial structures in the thermodynamic variables with horizontal scales of $\sim 5 - 20$km. Such structures are produced as localized signatures of individual convective elements, and are also

organized by the modest self-organization that occurs in the cloud field. The structures persist beyond the duration of the original element but decay over time. The heterogeneity in the thermodynamic fields then affects the triggering of convection on the next cycle and the local environment in which it develops. An explicit demonstration of the effects on convective development of thermodynamic structures at such scales (albeit motivated from a different argument) has been given in a numerical weather prediction context by Leoncini *et al.* (2010). Stirling and Petch (2004) also demonstrated the importance of spatial heterogeneity in thermodynamic fields in idealized, two-dimensional simulations. Various observational studies have also stressed the links between low-level thermodyanmic heterogeneity and deep convective initiation and development (e.g. Fabry 2006; Zhang and Klein 2010).

For the forcing timescales which exhibit variability in the cycle-integrated convection, the persistence of thermodynamic heterogeneity between cycles is clear, whereas at the diurnal and longer forcing timescales, such signatures of the convection from the previous cycle have almost vanished by the time the next cycle begins. The implication of this interpretation is that an understanding of small-scale thermodynamic signatures that appear in the aftermath of convective events, and the subsequent evolution of those signatures, would be needed for a complete, physically-well-founded parameterization of convective memory effects.

Acknowledgement

L. Davies was supported by the NERC award NER/S/A/2004/12408 with CASE support from the Met. Office.

References

Arakawa A. 2004. The cumulus parameterization problem: Past, present, and future. *J. Clim.* **17**: 2493–2525.

Arakawa A, Schubert WH. 1974. Interaction of a cumulus cloud ensemble with the large-scale environment. Part I. *J. Atmos. Sci.* **31**: 674–701.

Bechtold P, Köhler M, Jung T, Doblas-Reyes F, Leutbecher M, Rodwell MJ, Vitart F, Balsamo G. 2008. Advances in simulating atmospheric variability with the ECMWF model: From synoptic to decadal time-scales. *Quart. J. Roy. Met. Soc.* **134**: 1337–1351.

Bretherton CS, McCaa JR, Grenier H. 2004. A new parameterization for shallow cumulus convection and its application to marine subtropical cloud-topped boundary layers. Part I: Description and 1D results. *Mon. Wea. Rev.* **132**: 864–882.

Bretherton CS, Smolarkiewicz PK. 1997. Gravity waves, compensating subsidence and detrainment around cumulus clouds. *J. Atmos. Sci.* **46**: 740–759.

Cohen BG, Craig GC. 2004. The response time of a convective cloud ensemble to a change in forcing. *Quart. J. Roy. Meteor. Soc.* **130**: 933–944.

Cohen BG, Craig GC. 2006. Fluctuations in an equilibrium convective ensemble. Part II: Numerical experiments. *J. Atmos. Sci.* **63**: 2005–2015.

Daleu CL, Woolnough SJ, Plant RS. 2012. Cloud-resolving model simulations with one and two-way couplings via the weak-temperature gradient approximation. *To appear in: J. Atmos. Sci.* .

Davies L. 2008. Self organisation of convection as a mechanism for memory. PhD thesis, Department of Meteorology, University of Reading.

Davies L, Plant RS, Derbyshire SH. 2009. A simple model of convection with memory. *J. Geophys. Res.* **114**: D17 202.

Fabry F. 2006. The spatial variability of moisture in the boundary layer and its effect on convection initiation: Project-long characterisation. *Mon. Wea. Rev.* **134**: 79–91.

Gerard L, Geleyn JF. 2005. Evolution of a subgrid deep convection parametrization in a limited-area model with increasing resolution. *Quart. J. R. Meteorol. Soc.* **131**: 2293–2312.

Grandpeix JY, Lafore JP. 2010. A density current parameterization coupled to emanuel's convection scheme. Part I: The models. *J. Atmos. Sci.* **67**: 881–897.

Grant ALM, Brown AR. 1999. A similarity hypothesis for shallow-cumulus transports. *Quart. J. Roy. Met. Soc.* **125**: 1913–1936.

Gray MEB, Petch J, Derbyshire SH, Brown AR, Lock AP, Swann HA, Brown PRA. 2001. Version 2.3 of the Met Office Large Eddy Model: Part II. Scientific documentation. Technical report, Met Office.

Gregory D. 1997. The mass flux approach to the parameterization of deep convection. In: *The Physics and Parameterization of Moist Atmospheric Convection*, Smith RK (ed), Kluwer Academic Publishers, pp. 297–319.

Guichard F, Petch JC, Redelsperger JL, Bechtold P, ans S Cheinet JPC, Grabowski W, Grenier H, Jones CG, Köhler M, Piriou JM, Tailleux R, Tomasini M. 2004. Modelling the diurnal cycle of deep precipitating convection over land with cloud-resolving models and single-column models. *Quart. J. Roy. Meteor. Soc.* **130**: 3139–3172.

Jones TR. 2010. Quantifying the limits of convective parameterizations: A statistical characterization of simulated cumulus convection. Master's thesis, Department of Atmospheric Science, Colorado State University.

Jones TR, Randall DA. 2009. Quantifying the limits of convective parameterizations. *J. Geophys. Res.* **116**: D08 210.

Kain JS. 2004. The Kain–Fritsch convective parameterization: An update. *J. Appl. Meteorol.* **43**: 170–181.

Khairoutdinov M, Randall D. 2006. High-resolution simulation of shallow-to-deep convection transition over land. *J. Atmos. Sci.* **63**: 3421–3436.

Kuang Z. 2008. Modeling the interaction between cumulus convection and linear gravity waves using a limited-domain cloud system-resolving model. *J. Atmos. Sci.* **65**: 576–591.

LeMone MA, Zipser EJ, Trier SB. 1998. The role of environmental shear and thermodynamic conditions in determining the structure and evolution of mesoscale convective systems during TOGA COARE. *J. Atmos. Sci* **55**: 3493–3518.

Leoncini G, Plant RS, Gray SL, Clark PA. 2010. Perturbation growth at the convective scale for CSIP IOP18. *Q. J. R. Meteorol. Soc.* **136**: 653–670.

Manabe S, Smagorinsky JS, Strickler RF. 1965. A similarity hypothesis for shallow-cumulus transports. *Mon. Wea. Rev.* **93**: 769–798.

Mapes B, Neale R. 2011. Parameterizing convective organization. *Journal of Advances in Modeling Earth Systems* **3**(6).

Mapes BE. 1997. Equilibrium vs. activation controls on large–scale variations of tropical deep convection. In: *The Physics and Parameterization of Moist Atmospheric Convection*, Smith RK (ed), Kluwer Academic Publishers, pp. 321–358.

Marsham JH, Parker DJ. 2006. Secondary initiation of multiple bands of cumulonimbus over southern Britain. Part II: Dynamics of secondary initiation. *Quart. J. Roy. Meteor. Soc.* **132**: 1053–1072.

Pan DM, Randall DA. 1998. A cumulus parameterization with prognostic closure. *Quart. J. R. Meteorol. Soc.* **124**: 949–981.

Parodi A, Emanuel K. 2009. A theory for buoyancy and velocity scales in deep moist convection. *J. Atmos. Sci.* **66**: 3449–3463.

Petch JC. 2006. Sensitivity studies of developing convection in a cloud-resolving model. *Quart. J. Roy. Meteor. Soc.* **132**: 345–358.

Piriou JM, Redelsperger JL, amd J P Lafore JFG, Guichard F. 2007. An approach for convective parameterization with memory: Separating microphysics and transport in grid-scale equations. *J. Atmos. Sci.* **64**: 4127–4139.

Raymond D, Zeng X. 2005. Modelling tropical atmospheric convection in the context of the weak temperature gradient approximation. *Quart. J. R. Meteorol. Soc.* **131**: 1301–1320.

Rio C, Hourdin F, Grandpeix JY, Lafore JP. 2009. Shifting the diurnal cycle of parameterized deep convection over land. *Geophys. Res. Lett.* **36**: L07 809.

Robe FR, Emanuel KA. 2001. The effect of vertical wind shear on radiative-convective equilibrium states. *J. Atmos. Sci.* **58**: 1427–1445.

Rogers RR, Yau MK. 1989. *A short course in cloud physics*. Butterworth-Heinemann, 3rd edn.

Rotunno R, Klemp JB, Weisman ML. 1988. A theory for strong, long-lived squall lines. *J. Atmos, Sci.* **45**: 463–485.

Shutts GJ, Gray MEB. 1994. A numerical modelling study of the geostrophic adjustment process following deep convection. *Quart. J. Roy. Meteor. Soc.* **120**: 1145–1178.

Shutts GJ, Gray MEB. 1999. Numerical simulations of convective equilibrium under prescribed forcing. *Quart. J. R. Meteorol. Soc* **125**: 2767–2787.

Sobel AH, Bretherton CS. 2000. The cumulus parameterization problem: Past, present, and future. *J. Clim.* **13**: 4378–4392.

Stirling AJ, Petch JC. 2004. The impacts of spatial variability on the development of convection. *Quart. J. Roy. Meteor. Soc.* **130**: 3189–3206.

Tompkins AM. 2001. Organisation of tropical convection in low vertical wind shears: The role of cold pools. *J. Atmos. Sci.* **58**: 1650–1672.

Vallis GK, Shutts GJ, Gray MEB. 1997. Balanced mesoscale motion and stratified turbulence forced by convection. *Quart. J. Roy. Meteor. Soc.* **123**: 1621–1652.

Wagner TM, Graf HF. 2010. An ensemble cumulus convection parameterization with explicit cloud treatment. *J. Atmos. Sci.* **67**: 3854–3869.

Yang GY, Slingo J. 2001. The diurnal cycle in the tropics. *Mon. Wea. Rev.* **129**: 784–801.

Yano JI, Plant RS. 2012. Finite departure from convective quasi-equilibrium: Periodic cycle and discharge-recharge mechanism. *Quart. J. Roy. Met. Soc.* **128**: 626–637.

Zhang Y, Klein SA. 2010. Mechanisms affecting the transition from shallow to deep convcetion over land: Inferences from observations of the diurnal cycle collected at the ARM Souther Great Plains site. *J. Atmos. Sci.* **67**: 2943–2958.

Zimmer M, Graig GC, Wernli H, Keil C. 2011. Classification of precipitation events with a convective response timescale. *Geophys. Res. Lett.* **38**: L05 802.